

Received 11 July 2023, accepted 4 September 2023, date of publication 15 September 2023, date of current version 2 October 2023.

Digital Object Identifier 10.1109/ACCESS.2023.3315870

RESEARCH ARTICLE

Multi-UAV Collaboration and IMU Fusion Localization Method in Partial GNSS-Denied Scenarios

YI ZHENG^{1,2}, YAQIN XIE^{1,3}, AND JIAMIN LI^{1,2}, (Member, IEEE)

¹Changwang School of Honors, Nanjing University of Information Science and Technology, Nanjing 210044, China

²National Mobile Communications Research Laboratory, School of Information Science and Engineering, Southeast University, Nanjing 210096, China

³School of Electronic and Information Engineering, Nanjing University of Information Science and Technology, Nanjing 210044, China

Corresponding author: Yaqin Xie (xyq@nuist.edu.cn)

This work was supported in part by the National Natural Science Foundation of China (NSFC) under Grant 62001238; and in part by the Open Research Fund of National Mobile Communications Research Laboratory, Southeast University, under Grant 2022D11.

ABSTRACT When it comes to disaster rescue, quickly and accurately locating the trapped people will not miss the golden rescue time, thereby improving the success rate of rescue. The existing research has focused on the use of unmanned aerial vehicles (UAVs) to locate stationary user equipment (UE). However, the simultaneous movement of the UAVs and the UE brings about problems of UAV coordinate deviation and range interference, resulting in poor accuracy and stability of UE localization. To solve the mentioned issues above, a fusion localization method based on multi-UAV collaborative ranging and user-side inertial measurement unit (IMU) module was proposed for GNSS-denied scenarios. First, the initial coordinate deviations of the UAVs were corrected by multi-UAV collaboration; Then, a pre-processing scheme based on density peaks clustering (DPC) was proposed to eliminate the abnormal interference in the ranging data; Finally, the unscented Kalman filter (UKF) was used to realize the fusion localization based on multi-UAV ranging and user-side IMU module. The simulation results showed that the proposed scheme can maintain the accuracy and stability of UE localization in the presence of ranging interference, and the positioning error was reduced by 21.4% compared with the commonly used extended Kalman filter (EKF). Moreover, the proposed localization scheme had a better performance in low-altitude rather than high-altitude flight scenarios.

INDEX TERMS Density peaks clustering (DPC), fusion localization, inertial measurement unit (IMU), unmanned aerial vehicle (UAV), unscented Kalman filter (UKF).

I. INTRODUCTION

In emergency scenarios such as rescue for natural disasters and accidents, real-time location information of the rescuers and trapped people is particularly important for rescue work [1]. A precise location can speed up the response time of rescue teams and increase the chances of finding people trapped in critical situations. However, in the process of search and rescue, the affected areas are often faced with problems of satellite rejection and base station damage, which leads to interrupted communication links. Due to the absence of communication relays, users in the affected area

are generally unable to communicate with each other or with the outside world [2], and cannot obtain location information via the Internet or the Global Navigation Satellite System (GNSS). The traditional rescue often takes a blanket search for the missing person, which is aimless and easy to miss the golden rescue time. Therefore, it is extremely critical to provide an alternative localization solution for rescuers and trapped people in emergencies. In this article, the term ‘UAV’ refers to the unmanned aerial vehicle, and the term ‘UE’ refers to the user equipment.

The UAV airborne base stations (BS) have obvious advantages in search and rescue scenarios [3]. Without relying on ground infrastructure, UAVs can achieve dynamic network self-assembly by carrying small base stations

The associate editor coordinating the review of this manuscript and approving it for publication was Gianluca Cena¹.

and different sensors to enhance communication as well as localization services for affected areas and guarantee emergency handling capabilities [4]. For localization requirements, UAVs are often equipped with distance measurement modules such as time-of-flight (TOF) [5], [6], [7] or received signal strength indicator (RSSI) [8], [9] to obtain the distance information of the user equipment (UE). In addition, the UAV airborne base station has a certain flight altitude. On the one hand, it can avoid obstacles to receive satellite signals, and obtain its position information based on satellites. On the other hand, compared to ground base stations, it is easier to form Line of Sight (LOS) channels between UAV base stations and UEs [10], and both communication and ranging are more stable. So far, a team of UAVs can autonomously navigate, explore, detect, and find the target in a cluttered environment with a known map [11]. In December 2020, UAVs played a central role in the rescue of the largest mountain landslide in Norwegian history. DJI M300 RTK drones were used to quickly detect, obtain the target position, and guide the helicopter to rescue the trapped.

Recently, much research has concentrated on energy-efficient UAV path planning [12], [13] and area coverage [14], [15] for static UE localization. These works are based on two assumptions: accurate UAV coordinates and stationary UEs. However, the deviation of UAV coordinates may be accumulated during the movement of the UAVs. The UE positioning bias increases with UAV coordinate bias. Moreover, as the position of the UAVs and the UE is constantly changing, the signal may be blocked by an obstacle, leading to abnormal ranging data. This will result in large deviations or even failure of UE localization in a short time.

Aiming at the scene of partial GNSS-denied and the simultaneous movement of the UAVs and UEs, a localization scheme based on the fusion of multi-UAV and inertial measurement unit (IMU) was proposed to provide highly accurate and stable positioning services for the mobile UEs on the ground. The main contributions are summarized as follows.

- 1) A multi-UAV collaborative coordinate correction model was proposed and solved by the gradient descent method to eliminate the initial coordinate deviation of UAVs.
- 2) Aiming at the problem of ranging anomaly, a data screening method based on the Density Peaks Clustering (DPC) and multilateral matching degree was proposed, which can effectively eliminate abnormal data and enhance the stability of the localization algorithm.
- 3) Based on the unscented Kalman filter (UKF), a multi-UAV collaboration and user-side IMU module fusion localization algorithm was proposed. The simulation results showed that the positioning performance of the fusion localization scheme based on UKF is better than that of the extended Kalman filter (EKF), and achieved good robustness.

The rest of the article is structured as follows. Section II discusses the related works. Section III presents the

multi-UAV collaborative and IMU fusion localization model. In Section IV, the multi-UAV collaborative and IMU fusion localization algorithm is introduced from three aspects: UAV own coordinate correction, range data pre-processing, and UKF. The performance evaluation and analysis are presented in Section V. Finally, Section VI concludes the article with some future directions.

II. RELATED WORKS

The inertial navigation system (INS) [16] is a common scheme for mobile target localization, which can be used in both UAV and UE sides. INS uses the IMU module to obtain the acceleration and angular velocity, make real-time displacement estimations, and perform incremental positioning calculations. Owing to the advantages of low cost and short-term high accuracy, the fusion localization combined with the IMU module has been widely used in many scenarios such as inspection UAV positioning [17], vehicle positioning, and indoor pedestrian positioning [16]. With the miniaturization of the IMU module, it can be easily installed in mobile phones and other devices, thus enabling further extension to outdoor positioning scenarios and providing assisted navigation and localization services for mobile UEs.

High-precision UAV coordinates are primarily required for the UAV-based coordinate localization system. So far, most UAVs on the market use GNSS to obtain their coordinates. However, satellite-based UAV positioning cannot operate in dense urban environments or indoor environments [18]. Much work has been carried out on the cooperative localization for UAVs. In [17], the EKF was used to achieve the fusion positioning consisting of IMU, Ultra Wide Band (UWB), and optical flow. The multi-source fusion localization improved the accuracy and stability of individual inspection UAV positioning. W. Zhang et al. [20] proposed two improved schemes based on the particle swarm optimization (PSO) algorithm: hierarchical PSO (HPSO) and reference PSO (RPSO), which combined ground anchor deployment and multi-UAV relative position to realize the localization of UAV swarm. Both [17] and [20] required the advanced arrangement of static anchor nodes to assist in the coordinate acquisition of the UAVs, which is difficult to achieve when a disaster causes infrastructure damage. In [21] and [22], map-matching positioning was proposed to reduce the requirements for infrastructure but increased the hardware cost and computational complexity, which is particularly unfavorable for small UAVs with short endurance. Different from the idea of map matching, authors in [23] proposed a vision-based UAV group relative angle measurement scheme, which makes full use of the advantages of multi-device collaboration, and achieves a better UAV positioning effect than EKF. Multi-UAV collaboration can improve the positioning accuracy of individual UAVs, but once some of them have positioning anomalies, it would drag down the performance of the entire system. In [24], the proportion of

autonomous positioning of each UAV has adjusted adaptively, which improved the accuracy and stability of UAV group positioning. Multi-UAV joint networking brings about the problem of UAV formation control. References [25] and [26] realized the Leader-Following control from the perspective of velocity and heading angle control and simultaneous relative localization, respectively, which has a good reference for our work.

It can be seen that the EKF [17], [24], [27], [28] and PSO [20], [29], [30] algorithms are two commonly used cooperative localization algorithms. EKF uses the first-order Taylor expansion to approximate the distance equation, and the solution accuracy is limited [28]. Thanks to group learning, the PSO algorithm has the advantage of fast convergence, but the computational complexity is large [30]. In [20], authors reduced the computational complexity by flexibly reducing the number of particles, but the randomness of the particle initialization and iteration process still restricts the local search capability of the algorithm. When the analytic equation of the objective function is known, the gradient descent method [31] is more explicitly targeted and has a stronger local search capability and lower complexity than the PSO algorithm.

In complex environments, the UE ranging data obtained by UAV base stations can be partially abnormal due to signal interference, obstacle blockage, and other reasons. If the abnormal data can be filtered out, the influence can be eliminated from the root cause, to achieve more stable localization. In [32], the data anomaly was quantified as a time-varying path loss index, and a Newton gradient algorithm was proposed to solve the path loss index and distance estimation. However, this requires the use of redundancy in multilateral positioning, which means more UAVs are needed (more than needed for localization solving). This increases the cost of the equipment required for the emergency network. Aiming at the complex channel environment in the city, the three-dimensional map information was used to distinguish the RSSI ranging data obtained by LOS and Non-Line of Sight (NLOS) paths [33]. Then, the UAV path planning was optimized based on the path loss estimation. However, in the rescue scene, the surface situation may change significantly, and the three-dimensional map information needs to be re-collected. The above schemes mainly eliminated the influence of abnormal ranging data from the perspective of channel parameter estimation. In addition, it can also be considered from the perspective of data cleaning and screening. Different kinds of clustering methods are often used for data cleaning and screening. Among them, the division-based K-means clustering algorithm [34] is more suitable for finding clusters of convex data sets, but it needs to input the number of clusters in advance and is sensitive to noise and outliers, which is not suitable for noise removal. The Density-Based Spatial Clustering of Applications with Noise (DBSCAN) method [35] can effectively mark noise points and discover data clusters of any shape. However, the algorithm is very

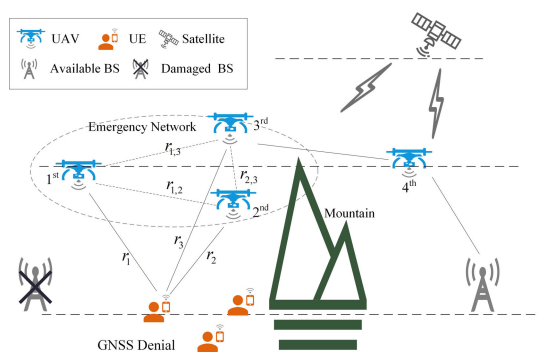


FIGURE 1. UAV emergency network based mobile UE localization system.

sensitive to user-defined parameters, and the parameter set can only be based on experience without regularity. Rodrigues et al. [36] further proposed the DPC algorithm in ‘Science’ in 2014, which reduced the number of user-defined parameters and significantly improved both clustering accuracy and computational efficiency. This efficient cluster identification clustering scheme can also be used in range data screening.

Research in indoor dynamic target localization provides a significant reference for outdoor localization. The range-based multilateral localization algorithms are relatively mature and can be easily solved via Newton’s iterative method [13], including the Chan-Taylor (CT) method [37], the gradient descent method [38], etc. However, the multilateral ranging method is essentially a single-source localization method, and the ranging information is prone to fluctuations, resulting in a large positioning deviation. In recent years, scholars have fused two or more localization technologies to improve the accuracy and stability of positioning [12], [39], [40]. In [39], the UWB ranging and IMU fusion positioning scheme based on EKF is used to improve localization accuracy in a small area. However, the EKF only uses the first-order Taylor approximation for the nonlinear system, which has a large error when the Taylor expansion center deviates significantly from the true value. To improve the accuracy of state estimation in nonlinear systems, S. J. Julier and J. K. Uhlmann [41] proposed the UKF algorithm. UKF uses Unscented Transform (UT) [42] to deal with the nonlinear transfer problem of mean and covet and approximates the probability density distribution of nonlinear functions. In [40], the fusion localization scheme based on UKF has been studied in indoor positioning and achieved better positioning results than EKF. This method can also be migrated to the localization of moving targets by multiple UAVs. However, the BS and the UE are moving simultaneously at this point, making the localization process more complex.

III. SYSTEM MODEL

The scenario of a mobile UE localization system based on emergency UAV networks is shown in Fig. 1. Due to the damage to the base station and the occlusion of the mountain,

TABLE 1. Index of notation.

Notation	Description
$\mathbf{p}_U(k)$	Coordinates of the user at time slot k
$\mathbf{p}_i(k)$	Coordinates of the i -th UAV at time slot k
$\mathbf{p}^{UAV}(k)$	Coordinates of all UAVs at time slot k
N	Number of UAVs
m	Number of user range measurements in a time slot
$r_i(k)$	The true distance between the i -th UAV and the user at time slot k
$r_{i,j}(k)$	Distance between the i -th UAV and the j -th UAV at time slot k
$\tilde{\mathbf{Z}}(k)$	The distance observation vector at time slot k
σ_r	The distance observation noise variance
$v_i(k)$	The distance observation noise between the i -th UAV and the user at time slot k
$\mathbf{v}(k)$	The observation noise vector at time slot k
$\mathbf{l}_i(k)$	The i -th measurement distance combination at time slot k
$\mathbf{L}(k)$	m sets of ranging data for the same target in k time slots
δ	Deviation between estimated and true values of user coordinates
Δt	The interval between two time slots
$\mathbf{X}(k)$	Mobile user's motion state vector at time slot k
$\mathbf{v}(k)$	Mobile user's velocity vector at time slot k
$\mathbf{a}(k)$	Mobile user's acceleration vector at time slot k
$\boldsymbol{\omega}_a(k)$	The process noise of acceleration at time slot k
σ_a	The variance of process noise rate
d_{ij}	Inter-element similarity in DPC
d_c	Cut-off distance in DPC
ρ_i	Local density of elements in DPC
δ_i	Relative distance of the elements in DPC
γ_i	The screening indicator in DPC
η	Decrease in cost function during gradient descent
$\boldsymbol{\omega}(k)$	The process noise vector at time slot k
λ	The scaling parameter for prediction error control
n_x	The dimension of $\mathbf{X}(k)$
$w_{mean}^{(i)}$	The weight of mean of the i -th sampling point
$w_{cov}^{(i)}$	The weight of covariance of the i -th sampling point
$\mathbf{P}_{Z_k Z_k}$	The observation covariance matrix at time slot k
$\mathbf{P}_{X_k Z_k}$	The cross-covariance matrix between the state vector and the observation vector at time slot k
$\mathbf{K}(k)$	The Kalman gain at time slot k
\mathbf{Q}	The covariance matrix of process noise
\mathbf{R}	The covariance matrix of observation noise
$\ \cdot\ $	The norm of a vector

GNSS in the UEs' area is invalid, so the UEs cannot obtain their location information. At this time, the UAV emergency network can be deployed around the UEs to be located. Because the UAV has a certain flight height, it can avoid occlusion and receive satellite signals. In the Figure, the 1st, 2nd, and 3rd UAVs are used as mobile anchors to provide localization and navigation services to ground users. The 4th UAV plays a relay role and connects the UAV emergency network to the ground base station, thus completing the network connection.

Section III discusses the localization system from three aspects: mobile UE localization based on UAV base station ranging, mobile UE self-positioning based on IMU, and multi-UAV collaborative coordinate correction. Subsequently, a complete multi-UAV collaborative and IMU fusion localization model was proposed. The meanings of the main symbols in this article are shown in Table 1.

A. MOBILE UE LOCALIZATION BASED ON UAV BASE STATION RANGING

During the emergency rescue process, both the UAVs and the rescue personnel are in motion. In this article, the continuous motion was discretized, and the time was divided according to the time slot. It is assumed that the position of the UAV and the UE does not change in each time slot.

The position of the ground UE at time slot k is

$$\mathbf{p}_U(k) = [x_U(k), y_U(k), 0]^T. \tag{1}$$

Similarly, the position of the i -th UAV at time slot k is

$$\mathbf{p}_i(k) = [x_i(k), y_i(k), z_i(k)]^T. \tag{2}$$

The real distance between the i -th UAV and the UE at time slot k is denoted as $r_i(k)$, and the distance relationship between the UE to be located and the i -th UAV can be obtained as

$$\|\mathbf{p}_i(k) - \mathbf{p}_U(k)\| = r_i(k). \tag{3}$$

The measured distance between the i -th UAV base station and the UE to be located is denoted as $\tilde{r}_i(k)$, containing the true distance $r_i(k)$ with the observation noise $v_i(k) \sim \mathcal{N}(0, \sigma_r^2)$. Let $\mathbf{v}(k) = [v_1(k), v_2(k), \dots, v_N(k)]^T$ denote the observation noise vector. The distance vector $\tilde{\mathbf{Z}}(k) = [\tilde{r}_1(k), \tilde{r}_2(k), \dots, \tilde{r}_N(k)]^T$ obtained from N UAV base stations is a function of the unknown quantity $\mathbf{p}_U(k)$:

$$\tilde{\mathbf{Z}}(k) = h(\mathbf{p}_U(k)) + \mathbf{v}(k), \tag{4}$$

where

$$h(\mathbf{p}_U(k)) = \begin{bmatrix} \|\mathbf{p}_1(k) - \mathbf{p}_U(k)\| \\ \|\mathbf{p}_2(k) - \mathbf{p}_U(k)\| \\ \vdots \\ \|\mathbf{p}_N(k) - \mathbf{p}_U(k)\| \end{bmatrix}.$$

The expression of the unknown quantity $\mathbf{p}_U(k)$ can be obtained by the inverse function as

$$\mathbf{p}_U(k) = h^{-1}(\tilde{\mathbf{Z}}(k) - \mathbf{v}(k)). \tag{5}$$

For a nonlinear function $h(\cdot)$, solving the analytic expression of its inverse function $h^{-1}(\cdot)$ is difficult, and a linear iterative approximation is generally used to obtain the numerical solution [21]. In this section, the Chan-Taylor method [37] is used to solve the numerical solution of $\mathbf{p}_U(k)$. First, the initial position $\mathbf{p}_U(k)$ of the iteration is obtained via Chan's method. The system of (6) is obtained by squaring both sides of (4):

$$\begin{cases} \|\mathbf{p}_1(k) - \mathbf{p}_U(k)\|^2 = \tilde{r}_1(k)^2 \\ \|\mathbf{p}_2(k) - \mathbf{p}_U(k)\|^2 = \tilde{r}_2(k)^2 \\ \vdots \\ \|\mathbf{p}_N(k) - \mathbf{p}_U(k)\|^2 = \tilde{r}_N(k)^2. \end{cases} \tag{6}$$

Taking the first equation in (6) as the base, the quadratic term is eliminated by difference, and $N - 1$ linear equations are obtained as shown in (7):

$$\mathbf{C}\mathbf{p}_U(k) = \mathbf{b}, \quad (7)$$

where

$$\mathbf{C} = \begin{bmatrix} \mathbf{p}_2(k)^T - \mathbf{p}_1(k)^T \\ \mathbf{p}_3(k)^T - \mathbf{p}_1(k)^T \\ \vdots \\ \mathbf{p}_N(k)^T - \mathbf{p}_1(k)^T \end{bmatrix}_{(N-1) \times 3}$$

$$\mathbf{b} = \frac{1}{2} \begin{bmatrix} \|\mathbf{p}_2(k)\|^2 - \|\mathbf{p}_1(k)\|^2 + \tilde{r}_1(k)^2 - \tilde{r}_2(k)^2 \\ \|\mathbf{p}_3(k)\|^2 - \|\mathbf{p}_1(k)\|^2 + \tilde{r}_1(k)^2 - \tilde{r}_3(k)^2 \\ \vdots \\ \|\mathbf{p}_N(k)\|^2 - \|\mathbf{p}_1(k)\|^2 + \tilde{r}_1(k)^2 - \tilde{r}_N(k)^2 \end{bmatrix}_{(N-1) \times 1}$$

While the mode of \mathbf{C} isn't equal to zero, that is to say, any three UAVs are not in a straight line, the coordinates of the UE can be obtained via the least square method:

$$\hat{\mathbf{p}}_U(k) = (\mathbf{C}^T \mathbf{C})^{-1} \mathbf{C}^T \mathbf{b}. \quad (8)$$

However, when the mode of \mathbf{C} is equal to 0, the linear correlation part should be removed and then obtain \mathbf{C}' for calculation.

Next, the Taylor series expansion is performed on (6) at $\hat{\mathbf{p}}_U(k)$, and the estimation error is reduced by cyclic iteration. The specific process of the Chan-Taylor method is as follows:

- 1) The relationship between the current user coordinate estimate $\hat{\mathbf{p}}_U(k)$ and the actual user coordinate $\mathbf{p}_U(k)$ can be expressed as

$$\mathbf{p}_U(k) = \hat{\mathbf{p}}_U(k) + \boldsymbol{\delta}. \quad (9)$$

where $\boldsymbol{\delta} = [\delta_x, \delta_y, \delta_z]^T$ denotes the deviation between the coordinate estimate $\hat{\mathbf{p}}_U(k)$ and the real position $\mathbf{p}_U(k)$ of the user.

- 2) Expand the system of (6) at $\hat{\mathbf{p}}_U(k)$ with a first-order Taylor series, and the linearized iterative equations are obtained as shown in (10):

$$\mathbf{M}_1 \boldsymbol{\delta} = \mathbf{M}_2, \quad (10)$$

where

$$\mathbf{M}_1 = \begin{bmatrix} \hat{\mathbf{p}}_U(k)^T - \mathbf{p}_1(k)^T \\ \hat{\mathbf{p}}_U(k)^T - \mathbf{p}_2(k)^T \\ \vdots \\ \hat{\mathbf{p}}_U(k)^T - \mathbf{p}_N(k)^T \end{bmatrix}_{N \times 3}$$

$$\mathbf{M}_2 = \frac{1}{2} \begin{bmatrix} \tilde{r}_1(k)^2 - \|\hat{\mathbf{p}}_U(k) - \mathbf{p}_1(k)\|^2 \\ \tilde{r}_2(k)^2 - \|\hat{\mathbf{p}}_U(k) - \mathbf{p}_2(k)\|^2 \\ \vdots \\ \tilde{r}_N(k)^2 - \|\hat{\mathbf{p}}_U(k) - \mathbf{p}_N(k)\|^2 \end{bmatrix}_{N \times 1}$$

The least squares solution of (10) is given by

$$\boldsymbol{\delta} = (\mathbf{M}_1^T \mathbf{M}_1)^{-1} \mathbf{M}_1^T \mathbf{M}_2. \quad (11)$$

- 3) Use $\hat{\mathbf{p}}_U(k) + \boldsymbol{\delta}$ instead of $\hat{\mathbf{p}}_U(k)$ and go back to step 1). Continue to calculate the corresponding deviation $\boldsymbol{\delta}$ and loop iterations to obtain the coordinate optimal estimate. The iteration is stopped when $\|\boldsymbol{\delta}\| < \varepsilon = 0.01$ or reaches the upper limit of the number of iterations. At this point the convergent solution $\mathbf{p}_U(k) = \hat{\mathbf{p}}_U(k)$ is obtained.

The Taylor iteration is an approximate Newton iteration with a clear objective and fast convergence. In the subsequent simulation experiments, the convergence solution can be obtained within 50 iterations. However, an upper limit on the number of iterations is still required in the case of a non-convex environment.

B. IMU-BASED MOBILE USER SELF-LOCALIZATION

Section III-B uses IMU sensors to obtain the motion status of the mobile user, which serves as an aid for positioning and improves system stability.

Denote the user's velocity vector at time slot k as

$$\mathbf{v}(k) = [v_x(k), v_y(k), v_z(k)]^T. \quad (12)$$

Similarly, the acceleration vector at time slot k is denoted as

$$\mathbf{a}(k) = [a_x(k), a_y(k), a_z(k)]^T. \quad (13)$$

The UE motion within each time slot is approximated as uniformly accelerated motion. As the sample period is Δt , the process noise of acceleration at time slot k is denoted as $\boldsymbol{\omega}_a(k)$, $\boldsymbol{\omega}_a(k) \sim \mathcal{N}(0, \sigma_a^2)$. After the integral of acceleration, the process noise of velocity and position is denoted as $\boldsymbol{\omega}_v(k)\Delta t$ and $\frac{\Delta t^2}{2}\boldsymbol{\omega}_a(k)$, respectively. Then, the UE's velocity $\mathbf{v}(k + 1)$ and position $\mathbf{p}_U(k + 1)$ at time slot $k + 1$ can be predicted by the motion state and acceleration of the target at time slot k are

$$\mathbf{v}(k + 1) = \mathbf{v}(k) + \mathbf{a}(k)\Delta t + \boldsymbol{\omega}_a(k)\Delta t \quad (14)$$

$$\mathbf{p}_U(k + 1) = \mathbf{p}_U(k) + \mathbf{v}(k)\Delta t + \frac{\Delta t^2}{2}\mathbf{a}(k) + \frac{\Delta t^2}{2}\boldsymbol{\omega}_a(k). \quad (15)$$

C. MULTI-UAV COLLABORATIVE POSITION CORRECTION

In the emergency network, the UAV base station can obtain its position information based on satellite signals. However, the built-in satellite navigation positioning module of the UAV has limited accuracy, with $\pm 1.5\text{m}$ deviation in the horizontal direction and $\pm 0.5\text{m}$ deviation in the vertical direction [19]. When the UAV base station system is unstable, the positioning error will be even larger, which will seriously affect the localization performance of the UAV-based network to ground users. To achieve high-precision localization of UE, multi-UAV collaboration can be used to correct the position information of UAVs.

The real distance between the i -th and j -th UAVs at time slot k is recorded as $r_{i,j}(k)$, then the distance relationship between the UAV base stations satisfies

$$\|\mathbf{p}_i(k) - \mathbf{p}_j(k)\| = r_{i,j}(k). \quad (16)$$

The distance measurement between the i -th and j -th UAV is denoted as $\tilde{r}_{i,j}(k)$, which can be obtained via RSSI, TOF, etc. N UAV base stations lead to $N(N - 1)/2$ equations:

$$\begin{cases} \|\mathbf{p}_1(k) - \mathbf{p}_2(k)\| = \tilde{r}_{1,2}(k) \\ \|\mathbf{p}_1(k) - \mathbf{p}_3(k)\| = \tilde{r}_{1,3}(k) \\ \vdots \\ \|\mathbf{p}_{N-1}(k) - \mathbf{p}_N(k)\| = \tilde{r}_{N-1,N}(k). \end{cases} \quad (17)$$

For the convenience of representation, the coordinates of all UAVs at time slot k are labeled as $\mathbf{P}_{UAV}(k) = [\mathbf{p}_1(k), \mathbf{p}_2(k), \dots, \mathbf{p}_n(k)]$. The GNSS coordinates of the UAVs are known and can be used as initial values, but further accuracy improvements are required. Thus, equation (17) can be rewritten as an optimization problem. The multi-UAV cooperative position correction model is expressed as follows:

$$\mathbf{P}_{UAV}(k) = \arg \min \sum_{i=1}^N \sum_{j=i+1}^N g(\mathbf{p}_i(k), \mathbf{p}_j(k), \tilde{r}_{i,j}(k)), \quad (18)$$

where

$$g(\mathbf{p}_i(k), \mathbf{p}_j(k), \tilde{r}_{i,j}(k)) = (\|\mathbf{p}_i(k) - \mathbf{p}_j(k)\| - \tilde{r}_{i,j}(k))^2.$$

In this paper, the GNSS coordinates of the UAV are used as the initial solution, and the gradient descent method is used to solve Equation (18). The specific solution process is given in IV-A.

D. MULTI-UAV COLLABORATION AND IMU FUSION LOCALIZATION MODEL

Combining III-A to III-C, the result of ranging and positioning the UE by the UAV base station is used as the coordinate observation $\tilde{\mathbf{p}}_U(k)$, while the coordinate prediction value obtained by the IMU module carried by the user itself is noted as $\hat{\mathbf{p}}_U(k + 1)$. The complete mobile UE multi-source localization model can be expressed as

$$\tilde{\mathbf{p}}_U(k) = h^{-1}(\tilde{\mathbf{Z}}(k) - \mathbf{v}(k)) \quad (19a)$$

$$\hat{\mathbf{p}}_U(k + 1) = \mathbf{p}_U(k) + \mathbf{v}(k)\Delta t + \frac{\Delta t^2}{2}\mathbf{a}(k) + \frac{\Delta t^2}{2}\boldsymbol{\omega}_a(k), \quad (19b)$$

where the UAV coordinates $\mathbf{P}_{UAV}(k)$ used as the positioning anchor point in $h^{-1}(\cdot)$ are obtained from (18).

Equations (19a) and (19b) correspond to the multi-UAV collaborative localization and user-side IMU localization processes, respectively, and the fusion algorithms for both will be presented in Section IV.

IV. MULTI-UAV COLLABORATION AND IMU FUSION LOCALIZATION ALGORITHM

The flow of the multi-UAV collaborative and IMU fusion localization algorithm is shown in Fig. 2. The algorithm was divided into three parts: first, the gradient descent method was proposed for UAV collaborative coordinate correction; Then, data screening based on DPC was performed to reduce the

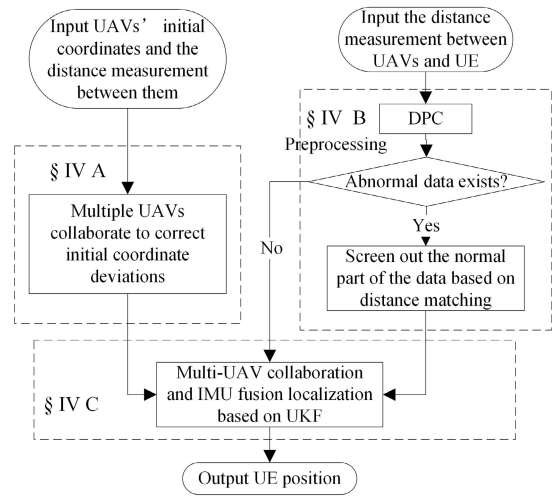


FIGURE 2. Process of multi-UAV collaboration and IMU fusion localization.

impact of abnormal data on UE localization accuracy; Finally, the multi-UAV collaborative and IMU fusion localization was realized based on UKF.

A. GRADIENT DESCENT METHOD TO CORRECT THE COORDINATES OF UAVs

The distance between UAV base stations is used as a constraint, and the gradient descent method is used to correct the initial UAV coordinates. The coordinates $\tilde{\mathbf{P}}_{UAV}(k)$, obtained by the UAV through satellite signal measurements, are used as the initial values. Then, construct the cost function according to (18):

$$G = \sum_{i=1}^N \sum_{j=i+1}^N g(\mathbf{p}_i(k), \mathbf{p}_j(k), \tilde{r}_{i,j}(k)). \quad (20)$$

Taking the first-order total differentiation of the UAV coordinates, the gradient expression is obtained as follows:

$$\overrightarrow{Grad} = \left[\frac{\partial G}{\partial \mathbf{p}_1(k)} \quad \frac{\partial G}{\partial \mathbf{p}_2(k)} \quad \dots \quad \frac{\partial G}{\partial \mathbf{p}_N(k)} \right]. \quad (21)$$

Since the gradient descent process needs to go through several iterations, the accuracy of the single gradient calculation is not required, and the approximation of the first-order partial derivatives can be obtained using the difference method.

Then, normalizing the gradient \overrightarrow{Grad} yields \overrightarrow{Grad}^* :

$$\overrightarrow{Grad}^* = \overrightarrow{Grad} / \|\overrightarrow{Grad}\|. \quad (22)$$

Set the step size to ξ and iteratively update the UAV coordinates:

$$\hat{\mathbf{P}}_{UAV}(k) = \tilde{\mathbf{P}}_{UAV}(k) + \xi \cdot \overrightarrow{Grad}^*. \quad (23)$$

The reduction of the updated cost function is denoted as η :

$$\eta = G|_{\mathbf{P}_{UAV}(k)=\hat{\mathbf{P}}_{UAV}(k)} - G|_{\mathbf{P}_{UAV}(k)=\tilde{\mathbf{P}}_{UAV}(k)}. \quad (24)$$

Determine whether the iterative process converges by the condition $|\eta| < \varepsilon = 0.01$. If it does not converge, let $\hat{\mathbf{P}}_{UAV}(k) = \tilde{\mathbf{P}}_{UAV}(k)$ and return to calculate \overrightarrow{Grad} based on (21). It is worth noting that when $\eta < 0$, it means that the optimal estimation point has been crossed after moving the step size ξ along the gradient direction. At this point, it is necessary to discount the step length ξ by half.

The process of the gradient descent method is shown in **Algorithm 1**.

Algorithm 1 The Gradient Descent Method for UAV Localization

Input: $\tilde{\mathbf{P}}_{UAV}(k), \tilde{r}_{i,j}(k)$

Output: $\hat{\mathbf{P}}_{UAV}(k)$

- 1: Set the variables: $\xi = 0.1, \varepsilon = 0.01$
- 2: **repeat**
- 3: Calculate \overrightarrow{Grad} based on (21)
- 4: Normalize \overrightarrow{Grad} to \overrightarrow{Grad}^*
- 5: $\hat{\mathbf{P}}_{UAV}(k) \leftarrow \tilde{\mathbf{P}}_{UAV}(k) + \xi \cdot \overrightarrow{Grad}^*$
- 6: Calculate η based on (24)
- 7: **if** $\eta < 0$ **then**
- 8: reduce ξ by half
- 9: **end if**
- 10: **until** $|\eta| < \varepsilon$
- 11: **return** Outputs

B. DATA PREPROCESSING BASED ON DPC

It is assumed that the UAV base station ranges the UE m times in the k -th time slot so that m sets of ranging data are obtained as $\mathbf{L}(k) = \{\mathbf{I}_1(k), \mathbf{I}_2(k), \dots, \mathbf{I}_m(k)\}$, where $\mathbf{I}_m(k)$ denotes the combination of the distances obtained from the m -th measurement by N UAVs in the k -th time slot.

When the range is normal, these data will float on either side of a reference value. If the base station range is abnormal, a portion of the data will deviate. Individual data anomalies show up as noisy points that deviate from the overall measurement distribution, while a larger number of data anomalies show up as independent cluster distributions. Therefore, a clustering method that can automatically identify cluster centers and noise points is needed.

The DPC algorithm [32] is an automatic cluster center identification method based on density peaks. The algorithm is based on the following two assumptions: one, the cluster centers are surrounded by other data points with lower density in the clusters. Two, the distance between cluster centers is relatively far. The inter-element similarity d_{ij} is obtained by

$$d_{ij} = \|\mathbf{I}_i(k) - \mathbf{I}_j(k)\|^2. \quad (25)$$

Then the similarity matrix \mathbf{D} is constructed as

$$\mathbf{D} = \begin{bmatrix} d_{11} & d_{12} & \cdots & d_{1m} \\ d_{21} & d_{22} & & \\ \vdots & & \ddots & \\ d_{m1} & d_{m2} & & d_{mm} \end{bmatrix}. \quad (26)$$

The local density ρ_i of the i -th element is obtain by

$$\rho_i = \sum_j \exp\left(-\frac{d_{ij}^2}{d_c^2}\right). \quad (27)$$

The relative distance δ_i of the i -th element is obtain by

$$\delta_i = \begin{cases} \min_{j: \rho_j > \rho_i} (d_{ij}), & \text{if } \exists j, \rho_j > \rho_i \\ \max_j (d_{ij}), & \text{otherwise.} \end{cases} \quad (28)$$

Then, a decision map is drawn to identify the points with larger local density ρ_i and relative distance δ_i as cluster centers. Subsequently, the non-centers are assigned to the nearest clusters. The cutoff distance d_c is the only parameter that needs to be set artificially for DPC. The set of points belonging to the cluster but not farther than d_c from other clusters is defined as the boundary region and the highest density point in the boundary region is defined as ρ_b . Finally, objects in the clusters with densities equal to or less than ρ_b are considered outliers (noise points) and are not counted in the clustering results.

However, the ‘‘large value’’ is only a qualitative description and there is no uniform standard, which causes the identification of cluster centers to be easily influenced by subjective factors. In response, [43] further proposed an improved DPC scheme that automatically selects clustering centers. Define the cluster center identification variable corresponding to the i -th element as

$$\gamma_i = \rho_i \times \delta_i. \quad (29)$$

Then, draw a descending graph by arranging γ_i in descending order. The slope between each adjacent point in the graph is then calculated and the data point with the largest change in slope is found as the critical point. The data point before the critical point is the center of clustering.

The specific execution of the DPC algorithm is shown in **Algorithm 2**.

Algorithm 2 Density Peaks Clustering

Input: $\mathbf{L}(k) = \{\mathbf{I}_1(k), \mathbf{I}_2(k), \dots, \mathbf{I}_m(k)\}$

Output: Cluster results

- 1: Set the variables: $d_c = 1$
- 2: Calculate the inter-element similarity d_{ij} and construct the similarity matrix \mathbf{D} based on (25) and (26) respectively
- 3: Calculating local density ρ_i , relative distance δ_i and cluster center identification variable γ_i based on (27) and (28) respectively
- 4: Calculate cluster center identification variable γ_i based on (29)
- 5: Identify cluster centers based on γ_i sequence
- 6: Assigning non-central points to the nearest high-density point cluster
- 7: Remove outliers with local density less than ρ_b
- 8: **return** Outputs

If multiple cluster centers are identified by DPC, this indicates the presence of an anomalous part of the data. To ensure localization accuracy, the UAV base station data cannot be deleted directly, and the normal part needs to be filtered out from it.

In response, Section IV-B proposed a multilateral matching degree-based screening scheme. Suppose $\mathbf{L}(k)$ is clustered by DPC to obtain $\{\boldsymbol{\varphi}_1, \dots, \boldsymbol{\varphi}_j, \dots, \boldsymbol{\varphi}_{n_c}\}$, a total of n_c central distributions, where $\boldsymbol{\varphi}_j = [\tilde{\varphi}_j^1, \tilde{\varphi}_j^2, \dots, \tilde{\varphi}_j^N]$, denoting the combination of N UAV-to-user range measurements. First, the Chan-Taylor method in Section III-A is used to find the user coordinate estimates $\hat{\mathbf{p}}_U^j(k)$, where $j = 1, 2, \dots, n_c$, corresponding to the above n_c range combinations. Then, the distance from $\hat{\mathbf{p}}_U^j(k)$ to each UAV base station $\|\hat{\mathbf{p}}_U^j(k) - \mathbf{p}_i(k)\|$ is calculated. Next, the distance calculation value is differenced from the measured value $\tilde{\varphi}_j^i$. Finally, the sum of squares of the differences is calculated to obtain the expression (30), which measures the multilateral matching degree.

$$E_j = \sum_{i=1}^N \left(\left\| \hat{\mathbf{p}}_U^j(k) - \mathbf{p}_i(k) \right\| - \tilde{\varphi}_j^i \right)^2 \quad (30)$$

The distance deviation degree E_j corresponding to each cluster center is derived according to (30), and the set $\boldsymbol{\varphi}_j$ with the smallest E_j among them is selected as the normal data combination so that the cleaning and screening of abnormal data are completed.

C. UNSCENTED KALMAN FILTER

Based on completing the UAV coordinate correction and ranging data preprocessing, Section IV-C combined the UAV base station ranging with the user-side IMU module based on unscented Kalman filter to achieve the UE localization. UKF depends on the assumption that both observed variables and state variables obey Gaussian distribution. The Gaussian distribution of random variables can be described by a set of sigma sampling points, and then the posterior mean and variance are approximated by the weighted statistical linear regression method through nonlinear function mapping. According to the conclusion of [42], compared with EKF, the estimation accuracy of UKF can reach the second-order accuracy of Taylor series expansion.

Use symbol $\mathbf{X}(k)$ to indicate the motion state of the UE in slot k :

$$\mathbf{X}(k) = [\mathbf{p}_U(k) \ \mathbf{v}(k)]^T. \quad (31)$$

where $\mathbf{p}_U(k)$ and $\mathbf{v}(k)$ are introduced in (1) and (12), respectively.

Let $\hat{\mathbf{X}}(k+1|k)$ denote the prediction of the state vector at time slot $k+1$. According to the recurrence relation of equation (14) and equation (15), the state equation can be expressed as follows:

$$\hat{\mathbf{X}}(k+1|k) = \mathbf{A}\hat{\mathbf{X}}(k) + \mathbf{B}\mathbf{a}(k) + \boldsymbol{\omega}(k), \quad (32)$$

Algorithm 3 UKF for UE Localization

Input: $\tilde{\mathbf{Z}}(k+1), \tilde{\mathbf{X}}(k|k), \mathbf{P}(k|k)$

Output: $\bar{\mathbf{X}}(k+1|k+1), \mathbf{P}(k+1|k+1)$

- 1: Set the variables: $\alpha = 1, \beta = 2, \kappa = 0$.
- 2: Calculate the sigma points

$$\mathbf{X}^{(i)}(k|k) = \left[\begin{array}{c} \bar{\mathbf{X}}(k) \\ \bar{\mathbf{X}}(k) + \sqrt{(n_x + \lambda) \mathbf{P}(k)} \\ \bar{\mathbf{X}}(k) - \sqrt{(n_x + \lambda) \mathbf{P}(k)} \end{array} \right]^T$$

- 3: Predict the sigma points and get the mean and covariance

$$\hat{\mathbf{X}}^{(i)}(k+1|k) = \mathbf{A}\mathbf{X}^{(i)}(k|k) + \mathbf{B}\mathbf{a}(k), \quad i = 0, 1, \dots, 2n_x$$

$$\bar{\mathbf{X}}(k+1|k) = \sum_{i=0}^{2n_x} w_m^{(i)} \hat{\mathbf{X}}^{(i)}(k+1|k)$$

$$\mathbf{P}(k+1|k) = \sum_{i=0}^{2n_x} w_c^{(i)} \left[\bar{\mathbf{X}}(k+1|k) - \hat{\mathbf{X}}^{(i)}(k+1|k) \right] \times \left[\bar{\mathbf{X}}(k+1|k) - \hat{\mathbf{X}}^{(i)}(k+1|k) \right]^T + \mathbf{Q}$$

- 4: Update sigma points

$$\mathbf{X}^{(i)}(k+1|k) = \left[\begin{array}{c} \bar{\mathbf{X}}(k+1|k) \\ \bar{\mathbf{X}}(k+1|k) + \sqrt{(n_x + \lambda) \mathbf{P}(k+1|k)} \\ \bar{\mathbf{X}}(k+1|k) - \sqrt{(n_x + \lambda) \mathbf{P}(k+1|k)} \end{array} \right]^T$$

- 5: Predict the observed values and calculate their mean and covariance

$$\hat{\mathbf{Z}}^{(i)}(k+1|k) = h(\mathbf{X}^{(i)}(k+1|k)), \quad i = 0, 1, \dots, 2n_x$$

$$\bar{\mathbf{Z}}(k+1|k) = \sum_{i=0}^{2n_x} w_m^{(i)} \hat{\mathbf{Z}}^{(i)}(k+1|k)$$

$$\mathbf{P}_{Z_k Z_k} = \sum_{i=0}^{2n_x} w_c^{(i)} \left[\bar{\mathbf{Z}}(k+1|k) - \hat{\mathbf{Z}}^{(i)}(k+1|k) \right] \times \left[\bar{\mathbf{Z}}(k+1|k) - \hat{\mathbf{Z}}^{(i)}(k+1|k) \right]^T + \mathbf{R}$$

$$\mathbf{P}_{X_k Z_k} = \sum_{i=0}^{2n_x} w_c^{(i)} \left[\bar{\mathbf{X}}(k+1|k) - \hat{\mathbf{X}}^{(i)}(k+1|k) \right] \times \left[\bar{\mathbf{Z}}(k+1|k) - \hat{\mathbf{Z}}^{(i)}(k+1|k) \right]^T$$

- 6: Calculate the Kalman gain and update the state

$$\mathbf{K}(k+1) = \mathbf{P}_{X_k Z_k} \mathbf{P}_{Z_k Z_k}^{-1}$$

$$\hat{\mathbf{X}}(k+1|k+1) = \bar{\mathbf{X}}(k+1|k) + \mathbf{K}_{k+1} \left[\tilde{\mathbf{Z}}(k+1) - \bar{\mathbf{Z}}(k+1) \right]$$

$$\mathbf{P}(k+1|k+1) = \mathbf{P}(k+1|k) + \mathbf{K}_{k+1} \mathbf{P}_{Z_k Z_k} \mathbf{K}_{k+1}^T$$

- 7: return Outputs

where

$$\mathbf{A} = \left[\begin{array}{cc} \mathbf{I}_{3 \times 3} & \Delta t \cdot \mathbf{I}_{3 \times 3} \\ \mathbf{O}_{3 \times 3} & \mathbf{I}_{3 \times 3} \end{array} \right]$$

$$\mathbf{B} = \left[\begin{array}{cc} \frac{1}{2} \Delta t^2 \cdot \mathbf{I}_{3 \times 3} & \Delta t \cdot \mathbf{I}_{3 \times 3} \end{array} \right]^T$$

$$\boldsymbol{\omega}(k) = \left[\begin{array}{cc} \frac{\Delta t^2}{2} \boldsymbol{\omega}_a(k) & \Delta t \boldsymbol{\omega}_a(k) \end{array} \right]^T.$$

Let $\tilde{\mathbf{Z}}(k+1)$ denote the observation vector at time slot $k+1$. According to equation (4), the observation equation can be expressed as:

$$\tilde{\mathbf{Z}}(k+1) = \begin{bmatrix} \|\mathbf{p}_U(k+1) - \mathbf{p}_1(k+1)\| \\ \|\mathbf{p}_U(k+1) - \mathbf{p}_2(k+1)\| \\ \vdots \\ \|\mathbf{p}_U(k+1) - \mathbf{p}_N(k+1)\| \end{bmatrix} + \mathbf{v}(k+1). \quad (33)$$

Then, let \mathbf{Q} and \mathbf{R} denote the covariance of the process noise $\boldsymbol{\omega}(k)$ and the observation noise $\mathbf{v}(k)$, respectively.

$$\mathbf{Q} = \text{diag}\left(\frac{1}{4}\sigma_a^2 \Delta t^4 \cdot \mathbf{1}_{1 \times 3} \quad \sigma_a^2 \Delta t^2 \cdot \mathbf{1}_{1 \times 3}\right) \quad (34)$$

$$\mathbf{R} = \sigma_r^2 \cdot \mathbf{I}_{N \times N} \quad (35)$$

In the Gaussian system, UKF uses a small number of sample points to obtain the distribution of variables after nonlinear transformation. The a priori mean $\bar{\mathbf{X}}(k)$ takes the value of the optimal estimate $\hat{\mathbf{X}}(k)$ of the current state vector. The set of sigma points obtained based on the prior mean and covariance matrix can be expressed as (36).

$$\begin{aligned} \mathbf{X}^{(0)}(k|k) &= \bar{\mathbf{X}}(k) \\ \mathbf{X}^{(i)}(k|k) &= \bar{\mathbf{X}}(k) + \left(\sqrt{(\lambda + n_x) \mathbf{P}(k|k)}\right)_i, \\ &\quad i = 1, \dots, n_x \\ \mathbf{X}^{(i)}(k|k) &= \bar{\mathbf{X}}(k) - \left(\sqrt{(\lambda + n_x) \mathbf{P}(k|k)}\right)_i, \\ &\quad i = n_x + 1, \dots, 2n_x \end{aligned} \quad (36)$$

where $\left(\sqrt{(\lambda + n_x) \mathbf{P}(k|k)}\right)_i$ represents the i -th column element of matrix $\left(\sqrt{(\lambda + n_x) \mathbf{P}(k|k)}\right)$. λ is the scaling factor to reduce the total prediction error, which is set to $\lambda = \alpha^2 (n_x + \kappa)$. n_x denotes the dimension of $\mathbf{X}(k)$. α is generally set to a small positive number to ensure the mean of the sigma points is around $\bar{\mathbf{X}}(k)$, the article takes $\alpha = 1$. Set the parameter $\kappa = 0$ to ensure that the matrix $(\lambda + n_x) \mathbf{P}(k|k)$ is a positive semi-definite matrix.

In the unscented transformation, the weight of the i -th sampling point in the calculation of the mean value is denoted as $w_{mean}^{(i)}$, and the weight in the calculation of the covariance is denoted as $w_{cov}^{(i)}$:

$$\begin{aligned} w_{mean}^{(0)} &= \frac{\lambda}{n_x + \lambda} \\ w_{cov}^{(0)} &= \frac{\lambda}{n_x + \lambda} + \left(1 - \alpha^2 + \beta^2\right) \\ w_{mean}^{(i)} &= w_{cov}^{(i)} = \frac{\lambda}{2(n_x + \lambda)}, \quad i = 1, 2, \dots, 2n_x, \end{aligned} \quad (37)$$

where β is a non-negative weight coefficient, $\beta = 2$.

Substitute the sigma point into the (32), predict the state mean $\bar{\mathbf{X}}(k+1|k)$ and the state covariance matrix $\mathbf{P}(k+1|k)$ at time slot $k+1$, and then generate new sigma points by the UT transformation. Substitute the new sigma points into (33) to calculate the $k+1$ step prediction mean $\bar{\mathbf{Z}}(k+1|k)$ of the system observation, and then calculate the

TABLE 2. Mean of UAV self-positioning errors.

Methods	X(m)	Y(m)	Horizon(m)	Height(m)
Collaboration	0.654	0.645	0.919	0.328
Kalman	0.89	0.902	1.267	0.328
Raw	1.2	1.2	1.697	0.4

observation covariance matrix $\mathbf{P}_{Z_k Z_k}$ and the cross-covariance matrix $\mathbf{P}_{X_k Z_k}$ between the state vector and the observation vector. Finally, calculate the Kalman gain according to the covariance and the state and update the covariance matrix at time slot $k+1$.

The specific unscented Kalman filter process is presented in Algorithm 3.

V. SIMULATION AND EXPERIMENTAL RESULTS

To verify the effectiveness of the proposed localization algorithm, we set three UAV base stations to form a typical UE localization scenario of the emergency network and use MATLAB to carry out simulation experiments. Both UAVs and UEs are equipped with IMU sensors. In the test region of $1000 \times 1000 \times 200 \text{ m}^3$, the UAV hovered at 150 m altitude according to the preset line to provide localization services for UEs on the ground. The coordinates of UAVs obtained via satellite navigation were set to have a deviation of $\pm 1.5 \text{ m}$ in the horizontal direction and $\pm 0.5 \text{ m}$ in the vertical direction [19]. Set the mean square deviation of the observation noise and the process noise to 1.5 and 0.2, respectively. The ranging error between the UAVs followed the distribution of $\mathcal{N}(0, 1^2)$. The root mean square error (RMSE) and the cumulative distribution function (CDF) were used to measure the localization accuracy and stability. First, the UAV cooperative coordinate correction algorithm was compared with the Kalman filter and the PSO algorithms. Then, the screening and cleaning effect of the preprocessing process was verified under range anomaly conditions. In addition, the performance of the UKF algorithm was compared with the EKF [39] and CT [37] algorithms under different conditions. Finally, the performance of the proposed multi-UAV collaborative IMU fusion localization algorithm in high-altitude and low-altitude scenarios was evaluated respectively.

A. PERFORMANCE OF UAV COLLABORATIVE CORRECTION

To verify the advantages of the UAV collaborative correction scheme proposed in this article, the commonly used Kalman method and the initial coordinates of the UAVs were used as a comparison. Table 2 shows the average localization errors of UAVs obtained by the three schemes. It can be seen that the two-dimensional accuracy of UAV coordinates obtained by using the UAV collaborative correction scheme proposed in this article was improved by about 45.8% compared with the initial UAV coordinates, and further improved by about 27.5% based on the commonly used Kalman filter. At the same time, the positioning accuracy of the proposed scheme in the vertical direction was not improved compared with the

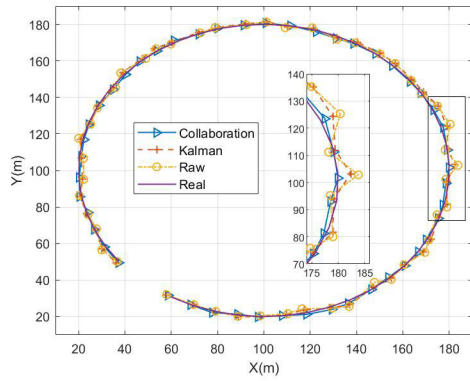


FIGURE 3. UAV tracking routes under different Correction schemes.

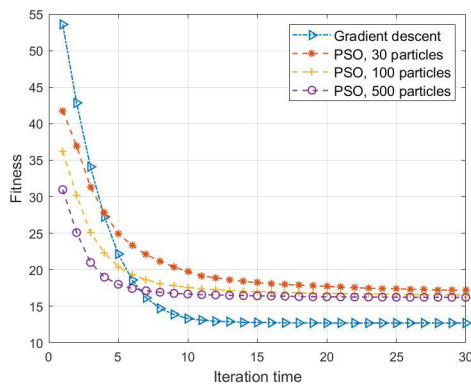


FIGURE 4. Comparison of iteration efficiency.

Kalman method. This is because many UAVs are almost at the same height, and the horizontal direction error is mainly corrected in the collaborative coordinate correction.

To more intuitively reflect the two-dimensional coordinate correction effect of the proposed scheme on UAV, the two-dimensional flight path diagram of the first UAV in the UAV network is drawn in Fig. 3. The results showed that both the UAV initial coordinate trajectory and the Kalman filtering trajectory have some deviations from the real UAV position, while the use of collaborative cointegration could effectively correct the two-dimensional deviation, which was more consistent with the real trajectory.

Fig. 4 compares the iterative efficiency of the gradient descent method and the commonly used PSO algorithm. It can be seen from this figure that with the increase in the number of particles, the PSO algorithm was more adaptable. Compared with the gradient descent method, the PSO algorithm achieved better fitness in the initial iteration. However, when the fitness was about 15, the PSO algorithm converged early and stopped optimization. In contrast, the gradient descent method with low complexity had fast convergence speed and good adaptability, which can meet the needs of UAV dynamic coordinate correction. Therefore, the gradient descent method was chosen in this paper instead of the PSO algorithm.

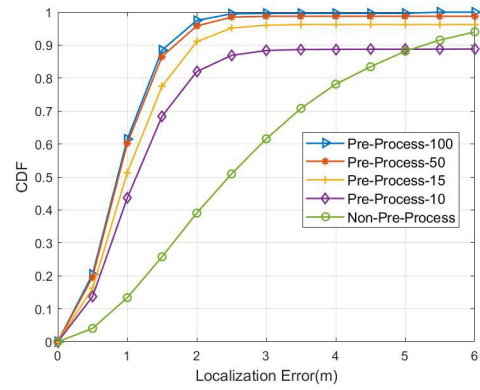


FIGURE 5. The effect of preprocessing for interference data.

B. PREPROCESSING PERFORMANCE IN THE CASE OF RANGING INTERFERENCE

Considering the influence of interference such as occlusion in the ranging process for UEs, Section V-B simulated the positioning of UE by adding outliers in the ranging data with a probability of 30%. The proposed data preprocessing scheme and the localization results without preprocessing were compared and analyzed under different data quantities. Moreover, the preprocessing effect on 10, 15, 50, and 100 sets of ranging data were tested respectively.

Fig. 5 compares the CDF of the localization errors with different data sizes. The results showed that when there was interference in user-ranging data, the localization deviation obtained without preprocessing was extremely large. For the proposed preprocessing scheme, the best localization effect was achieved when the data size was 100, and the positioning error of all test points was within 3 m. On a scale of 50, about 1% of the test points had positioning errors greater than 6m. If it is reduced to 15 ranging times, the probability of user positioning error greater than 6 m increases to 4%. When the number of measurements was further reduced to 10, the probability of user positioning error greater than 6 m was more than 10%. This is because as the number of measurements is reduced, insufficient data will lead to clustering anomalies in the preprocessing process, increasing the probability of screening failure.

When the amount of measured data is sufficient, the preprocessing scheme proposed in this article can eliminate almost all the effects of measured outliers. However, in the actual measurement process, because the UAV and the user are in the mobile state at the same time, a sufficient amount of data cannot be obtained. Therefore, it is inevitable that a small amount of abnormal data remains after preprocessing.

C. LOCALIZATION PERFORMANCE OF THE UKF-BASED FUSION ALGORITHM

Considering the scenario where the UAV base station and the UE move at the same time, the experiment first compared the localization effects of UKF, EKF, and CT methods under normal ranging conditions. Set the ground UEs to move along

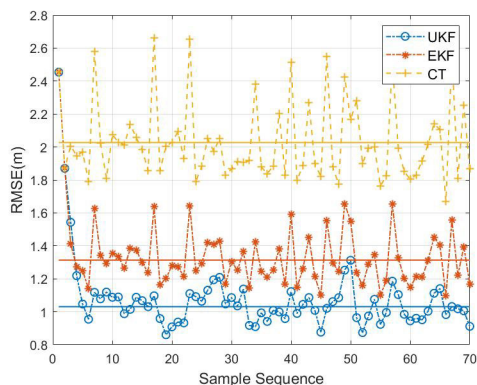


FIGURE 6. Localization error distribution of mobile UE sample sequence.

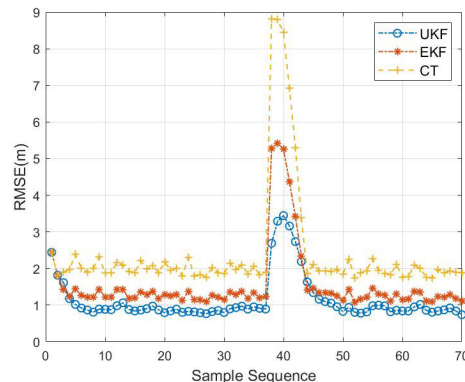


FIGURE 8. Filtering effect in abnormal residual scene.

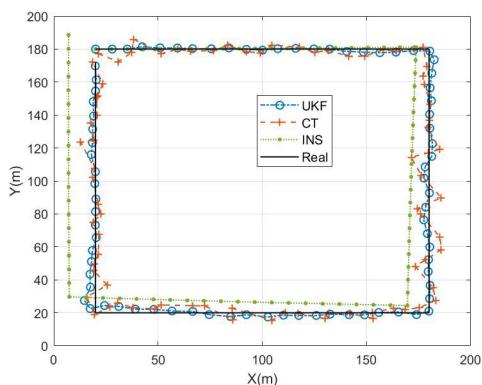


FIGURE 7. Trajectories of the mobile UEs.

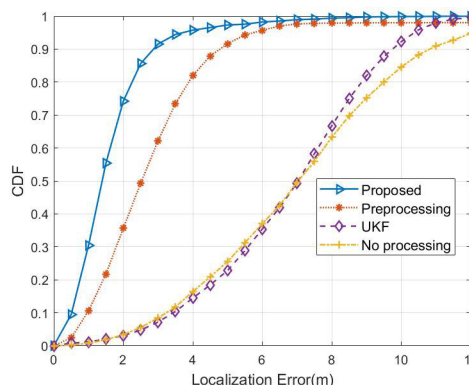


FIGURE 9. CDFs of localization error under interference conditions.

the known line, select 70 sample points on the way, and perform 100 rounds of testing.

Fig. 6 shows the RMSE distribution of the user at each sample point. It can be seen that the RMSE of the three localization algorithms near the starting point was not much different. With the recursive iteration, the UKF and EKF positioning errors gradually decrease and tended to be stable after 10 sample sequences. After iteration, the positioning error of UKF was about 1.03 m, while the positioning errors of EKF and CT were about 1.31 m and 2.03 m, respectively. The UE localization error has reduced by 21.4% compared with the commonly used EKF. Moreover, the time-consuming of UKF, EKF, and CT of each sample was about 1.7×10^{-5} s, 1.7×10^{-5} s and 2.1×10^{-5} s. It can meet the needs of dynamic UE localization.

To analyze the tracking effect of UKF on mobile users more intuitively, Fig. 7 shows the movement trajectories of one test user. Among them, due to the fluctuation of ranging information, the CT method based on single source ranging will lead to the deviation of some sample points. The positioning error of single-source inertial navigation based on the IMU module will accumulate with the increase of distance and deviate from the actual trajectory gradually. The UKF method based on multi-source location can eliminate some interference and avoid the error accumulation of the

IMU module, so the UE motion circuit is closer to the real path.

The experiment then compared and tested the localization of users by UKF, EKF, and CT when there are residual outliers. Select a part of the UE mobile line and set the ranging noise to $\mathcal{N}(0, 8^2)$ to simulate the influence of abnormal data residual on localization. The two-dimensional error distribution of moving UE sample points under abnormal conditions is obtained by 500 tests on the measurement data with abnormal residuals, as shown in Fig. 8. It can be seen that a residual measurement anomaly appeared near the 40th sample sequence. At this time, the RMSE of the CT method was close to 9 m after multiple experiments, which is a large deviation. However, the RMSE obtained by using the UKF was about 3.5 m, which can effectively reduce the influence of anomaly residual on location. Moreover, in the case of abnormal data, the localization accuracy of the UKF was still better than that of the EKF method. In Fig. 9, we compared the UE positioning error distribution of the preprocessing combined with the UKF scheme (the proposed scheme), only preprocessing, only UKF, and no processing when the data scale was 30. The experimental results showed that the scheme proposed achieved the best localization effect, in which the positioning error of about 96% of the sample points was less than 4 m, and that of all the sample points

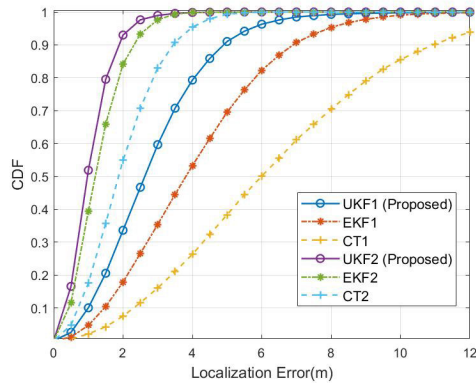


FIGURE 10. CDFs of localization error under high altitude and low altitude scenarios.

was less than 8 m, achieving excellent positioning accuracy and stability. When only preprocessing is used, there will be a small amount of abnormal residue, resulting in the CDF curve not reaching 100%. When only UKF is used, the correction effect is more obvious at large errors but even lower than the scheme without any treatment at small errors.

The preprocessing combined with the UKF filtering scheme proposed in this article can effectively eliminate the interference of ranging anomalies of localization for moving UEs. The simulation results verified that the proposed positioning scheme has good robustness.

D. LOCALIZATION PERFORMANCE IN HIGH-ALTITUDE AND LOW-ALTITUDE SCENARIOS

Due to the blocking of mountains, there are two localization strategies for the UAV emergency network: (1) The UAVs fly at high altitudes to obtain more accurate GNSS coordinates, which would mean poor range accuracy with the UEs. (2) The UAVs fly at low altitudes for more accurate ranging with the UEs, which would scarify certain GNSS accuracy for the UAVs. The error distribution of UAVs' GNSS coordinates was set to $\mathcal{N}(0, 1.5^2)$ and $\mathcal{N}(0, 9^2)$ for the high-altitude and low-altitude scenarios, respectively [19]. And the error distribution of the range between UAVs and UEs was set to $\mathcal{N}(0, 5^2)$ and $\mathcal{N}(0, 1^2)$ for the two scenarios, respectively [5].

In Fig. 10, the suffixes '1' and '2' in the legend correspond to the high-altitude scene and the low-altitude scene, respectively. It can be seen that the UKF method proposed was superior to the commonly used EKF and CT methods in both localization scenarios. For UKF positioning, more than 90% of the sample point positioning error was within 2 m in the low-altitude scene, while only less than 80% of the sample positioning error was less than 4 m in the high-altitude scene. This indicated that the positioning scheme proposed has a high tolerance for GNSS error at the UAV end, and is sensitive to ranging error with the UEs.

Table 3 shows the RMSE of the three localization schemes in high-altitude and low-altitude scenes, respectively.

TABLE 3. RMSE under high-altitude and low-altitude scenarios.

RMSE	UKF	EKF	CT
High altitude (m)	2.84	3.90	6.06
Low altitude (m)	1.41	1.65	2.37

Among them, the RMSE of UKF in the low altitude scene was only 1.41 m, while that in the high altitude scene was 2.84 m. This is because, as shown in subsection V-A, the synergy between UAVs effectively calibrates the original GNSS deviation. Therefore, in the actual localization process, the UAV flight height can be reduced, and scarify certain GNSS accuracy to obtain better positioning results for the UEs. Moreover, the multi-UAV collaboration and IMU fusion localization algorithm is also suitable for dynamic localization based on short-range IoT (Internet of Things).

However, since the proposed algorithm is sensitive to ranging error, a high-precision ranging module is needed to ensure localization accuracy in high-altitude scenarios. This will increase the power consumption and cost of the UAV system.

VI. CONCLUSION

Aiming at the problem of mobile UE localization in partial GNSS-denied scenarios, this article proposed a localization scheme based on multi-UAV collaboration and IMU fusion. Multiple UAVs are used to build an emergency network and integrate with the user-side IMU module to achieve high-precision UE localization. Thus, it can avoid the inefficient traditional blanket search and improve rescue efficiency. First, a multi-UAV collaborative correction model was proposed, and the gradient descent method was used to correct the initial coordinates of the UAV. Then, a data filtering method based on DPC was proposed to reduce the impact of abnormal data on localization. On this basis, a multi-UAV collaborative and IMU fusion localization algorithm based on UKF was proposed. The simulation results showed that the proposed UAV collaborative coordinate correction algorithm can effectively improve the two-dimensional coordinate accuracy of UAV; The RMSE of the proposed UKF method has reduced by 21.4% compared with the commonly used EKF method; Under interference conditions, the proposed scheme can still achieve high-precision and high-stability UE localization, and has good robustness; The proposed scheme is tolerant to GNSS deviation at the UAV end but sensitive to ranging noise with the UEs, so it is more suitable for low-altitude flight localization scenarios. Moreover, the multi-UAV collaboration and IMU fusion localization algorithm can also apply to short-range dynamic IoT localization.

It is worth noting that in addition to the flight height, dense forests and buildings will also seriously reduce the ranging accuracy, thus affecting the accuracy of the localization scheme proposed in this paper. In practical rescue

applications, personnel positioning is only the first step. The UAV emergency network also needs to guarantee tasks such as communication and environmental awareness. In the future, we will further study the channel sensing of UAV base stations in complex obstacle environments.

REFERENCES

- [1] R. Ravichandran, D. Ghose, and K. Das, "UAV based survivor search during floods," in *Proc. Int. Conf. Unmanned Aircr. Syst. (ICUAS)*, Atlanta, GA, USA, Jun. 2019, pp. 1407–1415.
- [2] K. Mase, "How to deliver your message from/to a disaster area," *IEEE Commun. Mag.*, vol. 49, no. 1, pp. 52–57, Jan. 2011.
- [3] Z. Gong, C. Li, F. Jiang, R. Su, R. Venkatesan, C. Meng, S. Han, Y. Zhang, S. Liu, and K. Hao, "Design, analysis, and field testing of an innovative drone-assisted zero-configuration localization framework for wireless sensor networks," *IEEE Trans. Veh. Technol.*, vol. 66, no. 11, pp. 10322–10335, Nov. 2017.
- [4] W. Li, W. Qing, X. Lianming, S. Yuan, Z. Ping, and F. Aiguo, "Research on low-energy-consumption deployment of emergency UAV network for integrated communication-navigating-sensing," *J. Commun.*, vol. 43, no. 7, pp. 1–20, Jul. 2022.
- [5] R. M. Rao, A. V. Padaki, B. L. Ng, Y. Yang, M.-S. Kang, and V. Marojevic, "ToA-based localization of far-away targets: Equi-DOP surfaces, asymptotic bounds, and dimension adaptation," *IEEE Trans. Veh. Technol.*, vol. 70, no. 10, pp. 11089–11094, Oct. 2021.
- [6] Y. Kang, Q. Wang, J. Wang, and R. Chen, "A high-accuracy TOA-based localization method without time synchronization in a three-dimensional space," *IEEE Trans. Ind. Informat.*, vol. 15, no. 1, pp. 173–182, Jan. 2019.
- [7] S. Zhao, X.-P. Zhang, X. Cui, and M. Lu, "A new TOA localization and synchronization system with virtually synchronized periodic asymmetric ranging network," *IEEE Internet Things J.*, vol. 8, no. 11, pp. 9030–9044, Jun. 2021.
- [8] J. Zhu, P. Hou, K. Nagayama, Y. Hou, S. Denno, and R. Ferdian, "Two-dimensional RSSI-based indoor localization using multiple leaky coaxial cables with a probabilistic neural network," *IEEE Access*, vol. 10, pp. 21109–21119, 2022.
- [9] H.-C. Yen, L.-Y. Ou Yang, and Z.-M. Tsai, "3-D indoor localization and identification through RSSI-based angle of arrival estimation with real Wi-Fi signals," *IEEE Trans. Microw. Theory Techn.*, vol. 70, no. 10, pp. 4511–4527, Oct. 2022.
- [10] S. G. Sanchez, S. Mohanti, D. Jaisinghani, and K. R. Chowdhury, "Millimeter-wave base stations in the sky: An experimental study of UAV-to-ground communications," *IEEE Trans. Mobile Comput.*, vol. 21, no. 2, pp. 644–662, Feb. 2022.
- [11] X. Zhu, F. Vanegas, F. Gonzalez, and C. Sanderson, "A multi-UAV system for exploration and target finding in cluttered and GPS-denied environments," in *Proc. Int. Conf. Unmanned Aircr. Syst. (ICUAS)*, Athens, Greece, Jun. 2021, pp. 721–729.
- [12] B. Yuan, R. He, B. Ai, R. Chen, G. Wang, J. Ding, and Z. Zhong, "A UAV-assisted search and localization strategy in non-line-of-sight scenarios," *IEEE Internet Things J.*, vol. 9, no. 23, pp. 23841–23851, Dec. 2022.
- [13] M. Atif, R. Ahmad, W. Ahmad, L. Zhao, and J. J. P. C. Rodrigues, "UAV-assisted wireless localization for search and rescue," *IEEE Syst. J.*, vol. 15, no. 3, pp. 3261–3272, Sep. 2021.
- [14] Y.-C. Du, M.-X. Zhang, H.-F. Ling, and Y.-J. Zheng, "Evolutionary planning of multi-UAV search for missing tourists," *IEEE Access*, vol. 7, pp. 73480–73492, 2019.
- [15] L. Ruan, J. Wang, J. Chen, Y. Xu, Y. Yang, H. Jiang, Y. Zhang, and Y. Xu, "Energy-efficient multi-UAV coverage deployment in UAV networks: A game-theoretic framework," *China Commun.*, vol. 15, no. 10, pp. 194–209, Oct. 2018.
- [16] F. Potorti, J. Torres-Sospedra, D. Quezada-Gaibor, A. R. Jiménez, F. Seco, A. Pérez-Navarro, M. Ortiz, N. Zhu, V. Renaudin, R. Ichikari, and R. Shimomura, "Off-line evaluation of indoor positioning systems in different scenarios: The experiences from IPIN 2020 competition," *IEEE Sensors J.*, vol. 22, no. 6, pp. 5011–5054, Mar. 2022.
- [17] J. Ji, X. Sun, and W. Zhou, "Application of multi-source fusion localization algorithm in inspection UAV," *J. Navigat. Positioning*, vol. 10, no. 4, pp. 130–137, 2022.
- [18] S. Hacoheh, O. Medina, T. Grinshpoun, and N. Shvalb, "Improved GNSS localization and Byzantine detection in UAV swarms," *Sensors*, vol. 20, no. 24, p. 7239, 2020.
- [19] *MATRICE 600 UAV Specifications*. Accessed: Apr. 1, 2020. [Online]. Available: <https://www.dji.com/es/matrice600/info>
- [20] W. Zhang and W. Zhang, "An efficient UAV localization technique based on particle swarm optimization," *IEEE Trans. Veh. Technol.*, vol. 71, no. 9, pp. 9544–9557, Sep. 2022.
- [21] S. Minaeian, J. Liu, and Y.-J. Son, "Vision-based target detection and localization via a team of cooperative UAV and UGVs," *IEEE Trans. Syst., Man, Cybern., Syst.*, vol. 46, no. 7, pp. 1005–1016, Jul. 2016.
- [22] J. Zhuang, X. Chen, M. Dai, W. Lan, Y. Cai, and E. Zheng, "A semantic guidance and transformer-based matching method for UAVs and satellite images for UAV geo-localization," *IEEE Access*, vol. 10, pp. 34277–34287, 2022.
- [23] D. Wang, B. Lian, Y. Liu, and B. Gao, "A cooperative UAV swarm localization algorithm based on probabilistic data association for visual measurement," *IEEE Sensors J.*, vol. 22, no. 20, pp. 19635–19644, Oct. 2022.
- [24] D. Shi, C. Liu, and F. She, "Cooperation localization method based on location confidence of multi-UAV in GPS-denied environment," *Comput. Sci.*, vol. 49, no. 4, pp. 302–311, Apr. 2022.
- [25] Y. Xu, J. Wang, J. Wang, and Y. Ke, "Nonlinear formation control of small fixed-wing UAVs with velocity and heading rate constraints," in *Proc. IEEE Int. Conf. Mechatronics Autom. (ICMA)*, Changchun, China, Aug. 2018, pp. 1275–1280.
- [26] T.-M. Nguyen, Z. Qiu, T. H. Nguyen, M. Cao, and L. Xie, "Distance-based cooperative relative localization for leader-following control of MAVs," *IEEE Robot. Autom. Lett.*, vol. 4, no. 4, pp. 3641–3648, Oct. 2019.
- [27] M. M. Zhou, B. Zhang, and Q. Zhao, "Cooperative localization algorithm based on adaptive fading Sage–Husa extended Kalman filter," *Chin. J. Ship Res.*, vol. 17, no. 4, pp. 92–97, 2022.
- [28] F. Hu and G. Wu, "Distributed error correction of EKF algorithm in multi-sensor fusion localization model," *IEEE Access*, vol. 8, pp. 93211–93218, 2020.
- [29] Z.-H. Zhan, J. Zhang, Y. Li, and Y.-H. Shi, "Orthogonal learning particle swarm optimization," *IEEE Trans. Evol. Comput.*, vol. 15, no. 6, pp. 832–847, Dec. 2011.
- [30] M. Y. Arafat and S. Moh, "Localization and clustering based on swarm intelligence in UAV networks for emergency communications," *IEEE Internet Things J.*, vol. 6, no. 5, pp. 8958–8976, Oct. 2019.
- [31] H. Xie, F. Wang, Q. Xun, Y. He, J. Rodríguez, and R. Kennel, "A low-complexity gradient descent solution with backtracking iteration approach for finite control set predictive current control," *IEEE Trans. Ind. Electron.*, vol. 69, no. 5, pp. 4522–4533, May 2022.
- [32] X. Zou, F. Zhou, L. Fan, and W. Chen, "Shadowing cancellation and iterative Newton-gradient algorithm for UAV-assisted localization," *IEEE Commun. Lett.*, vol. 25, no. 11, pp. 3570–3574, Nov. 2021.
- [33] O. Esrafilian, R. Gangula, and D. Gesbert, "Three-dimensional-map-based trajectory design in UAV-aided wireless localization systems," *IEEE Internet Things J.*, vol. 8, no. 12, pp. 9894–9904, Jun. 2021.
- [34] J. Qi, Y. Yu, L. Wang, and J. Liu, "K*-means: An effective and efficient K-means clustering algorithm," in *Proc. IEEE Int. Conferences Big Data Cloud Comput. (BDCloud), Social Comput. Netw. (SocialCom), Sustain. Comput. Commun. (SustainCom) (BDCloud-SocialCom-SustainCom)*, Atlanta, GA, USA, Oct. 2016, pp. 242–249.
- [35] A. K. M. R. Chowdhury, Md. E. Mollah, and Md. A. Rahman, "An efficient method for subjectively choosing parameter 'k' automatically in VDBSCAN (varied density based spatial clustering of applications with noise) algorithm," in *Proc. 2nd Int. Conf. Comput. Autom. Eng. (ICCAE)*, vol. 1, Singapore, Feb. 2010, pp. 38–41.
- [36] A. Rodriguez and A. Laio, "Clustering by fast search and find of density peaks," *Science*, vol. 344, no. 6191, pp. 1492–1496, Jun. 2014.
- [37] P. Wang and N. Zhang, "A cooperative location method based on chan and Taylor algorithms," *Appl. Mech. Mater.*, vols. 20–23, pp. 565–569, Jan. 2010.
- [38] S. Zhang, Y. Qi, and H. Lv, "UWB positioning optimization method based on redundant distance screening," *J. Tsinghua Univ.*, vol. 62, no. 5, pp. 934–942, 2022.
- [39] L. Xie, X. Liu, and Y. Wang, "Indoor EKF localization algorithm based on RFID carrier phase," in *J. Commun.*, vol. 43, no. 3, pp. 124–134, Mar. 2022.

- [40] D. Feng, C. Wang, C. He, Y. Zhuang, and X.-G. Xia, "Kalman-filter-based integration of IMU and UWB for high-accuracy indoor positioning and navigation," *IEEE Internet Things J.*, vol. 7, no. 4, pp. 3133–3146, Apr. 2020.
- [41] S. Julier and J. K. Uhlmann, "A general method for approximating nonlinear transformations of probability distributions," Dept. Eng. Sci., Univ. Oxford, Oxford, U.K., Tech. Rep. RRG, Nov. 1996.
- [42] S. Wang, Y. Lyu, and W. Ren, "Unscented-transformation-based distributed nonlinear state estimation: Algorithm, analysis, and experiments," *IEEE Trans. Control Syst. Technol.*, vol. 27, no. 5, pp. 2016–2029, Sep. 2019.
- [43] Z. Wang, "Research on density peak clustering algorithm by automatically determining," M.S. thesis, School Comput. Sci. Technol., Xidian Univ., Xi'an, China, 2020.



YI ZHENG is currently pursuing the B.S. degree in communication engineering with the Changwang School of Honors, Nanjing University of Information Science and Technology. His research interests include UAV localization and routing planning.



YAQIN XIE received the Ph.D. degree in communication and information systems from Southeast University, in 2011. Then, she joined the School of Electronic and Information Engineering, Nanjing University of Information Science and Technology. From February 2015 to February 2016, she was supported by the National Study Fund to visit the King's College London, U.K., as a Visiting Scholar. Her current research interests include indoor localization, satellite navigation, routing planning, and artificial Intelligence.



JIAMIN LI received the B.S. and M.S. degrees in communication and information systems from Hohai University, Nanjing, China, in 2006 and 2009, respectively, and the Ph.D. degree in information and communication engineering from Southeast University, Nanjing, in 2014. He joined the National Mobile Communications Research Laboratory, Southeast University, in 2014, where he has been an Associate Professor, since 2019. His research interests include massive MIMO, distributed antenna systems, and multi-objective optimization.

...